Journal of
Materials Chemistry A

ARTICLE

Received 00th January 20xx,
Accepted 00th January 20xx

DOI: 10.1039/x0xx00000x

www.rsc.org/

Fabrication of Robust Superhydrophobic Surfaces via Aerosol-Assisted CVD and Thermo-Triggered Healing of Superhydrophobicity by Recovery of Roughening Structures

Xiao-Jing Guo, [a, b] Chao-Hua Xue,[*, a, c] Sanjayan Sathasivam, [b] Kristopher Page,[b] Guanjie He,[b] Jian Guo, [b] Premrudee Promdet,[b] Frances L. Heale,[b] Claire J. Carmalt,[b] and Ivan P. Parkin[*, b]

Artificial self-healing superhydrophobic surfaces have become a new research hotspot from their recoverable non-wetting performances and practical perspective. In this paper, superhydrophobic surface was fabricated by aerosol-assisted layer-by-layer chemical vapor deposition (AA-LbL-CVD) of epoxy resin and PDMS polymer films. The obtained samples showed excellent chemical robustness even after longtime exposure to pH solution and UV light irradiation as well as great mechanical stability against sandpaper abrasion and double-sided tape peeling. Importantly, due to the shape memory effect of the polymer films, the as-prepared samples could recover the previously crushed micro-nano structures by heat treatment to make the surface superhydrophobic, showing thermo-triggered healing of superhydrophobicity.

Introduction

Nature inspired superhydrophobic surfaces have attracted tremendous attention due to their significant applications, such as oil-water separation,[1-5] anti-fouling,[6,7] anti-icing,[8-12] self-cleaning[13-17] and corrosion resistance.[18-20] It is generally known that such surfaces can be obtained by combining hierarchical micro-nano roughness structures with low surface energy materials.[21-23] However, superhydrophobic surfaces easily lose their superhydrophobicity owing to the damage of the rough structures and low surface energy chemical composition in practical applications. Recently, to overcome these disadvantages, artificial self-healing superhydrophobic surfaces have become a new research focus due to their recoverable non-wetting performances and wide applications, in which the self-healing ability can be realized by restoring both hierarchical roughness structure and surface chemistry.

Numerous self-healing superhydrophobic surfaces have been prepared on different substrates using various methods/techniques.[24-28] An early report on self-healing superhydrophobic surfaces described the preparation via layer-by-layer assembly of polyelectrolyte complexes of poly(allylamine hydrochloride) (PAH), sulfonated poly(ether ether ketone) (SPEEK) and poly(acrylic acid) (PAA) on the substrate to form porous coatings with micro- and nano-scaled hierarchical structures.[29] These polymeric porous coatings could preserve and facilitate the migration of low surface energy species when the surface lost its superhydrophobicity due to partial decomposition of low surface energy materials. Self-healing superhydrophobic fabrics have been made by coating the fiber surfaces with a hydrolysis product from fluorinated-decyl polyhedral oligomeric silsesquioxane (FD-POSS) and a fluorinated alkyl silane (FAS).[30] Upon damaging the surface chemically, polar groups were introduced, resulting in reduced surface hydrophobicity. However, molecular rotation and movement of fluorinated alkyl chains resulted in FD-POSS/FAS coated fabrics with self-healing properties and recovery of superhydrophobicity under heating. In addition, superhydrophobic surfaces were also prepared by coating of polystyrene/SiO_2 core/shell structural nanoparticles and polydimethylsiloxane.[31] With the release of hydrophobic polystyrene, the surface could be automatically restored in 12 h at room temperature or by heat curing and tetrahydrofuran treatment after damaging by air plasma treatment. Clearly, the self-healing ability of these superhydrophobic surfaces was achieved by providing the damaged surface with low surface energy substances that were preserved in advance in the interior of the carrier materials.

[a] College of Environmental Science and Engineering, Shaanxi University of Science and Technology, Xi'an 710021, China

[b] Department of Chemistry, University College London, London, WC1H 0AJ, United Kingdom

[c] College of Bioresources Chemical and Materials Engineering, Shaanxi University of Science and Technology, Xi'an 710021, China

E-mail: xuech@zju.edu.cn, i.p.parkin@ucl.ac.uk

† Electronic supplementary information (ESI) available.

In addition to "the migration of low surface energy substances" strategy, self-healing superhydrophobic surfaces can also be obtained by self-repair of su rface micro-nano tier roughness structure. Self-healing superhydrophobic porous polymer films were fabricated via layer-by-layer assembly of branched poly(ethyleneimine) and poly(vinyl-4,4-dimethylazlac-tone).[32] The as-prepared film can not only sustain superhydrophobicity after physical erosion but can also fully recover superhydrophobicity using a water-assisted approach after the film was severely crushed. Chen *et al* fabricated self-healing superhydrophobic surfaces based on the mixing of polystyrene (PS), fluorinated SiO_2 nanoparticles, hydrophobic poly(fluoro)siloxane binder and photocatalytic TiO_2 nanoparticles (P25).[33] When the surface roughness structure was mechanically damaged, the surface structure could be reconstructed and the superhydrophobicity could be recovered after UV irradiation. In another method, the self-healing superhydrophobic surfaces were prepared by the self-organization of colloidal particles at interfaces under annealing with a mixture of perfluorinated wax/colloidal silica particles.[34] Das et al.[35] demonstrated a superhydrophobic bulk coating by using the 1,4-conjugate addition reaction between aliphatic primary amine and aliphatic acrylate groups for the appropriate and covalent integration of a modified-graphene oxide nanosheet which could restore its superhydrophobic properties after releasing the pressure by recovering the hierarchical topography. Although these results were desirable, most of the fabrication processes are time-consuming and too complicated for practical applications. In comparison to "the migration of low surface materials" strategy, the recovery of surface roughness structure to impart surface self-healing ability still faces great challenges.

Shape memory polymers (SMPs) are a class of intelligent materials which have the ability of recovery their original shape (permanent shape) from a temporary shape when they are exposed to an appropriate stimulus such as heat, light, electric field, magnetic field or moisture.[36-40] Typically, a shape memory programming cycle includes the follow steps: first, the SMP is heated above its phase transition temperature, deformed and fixed by an external force. Secondly the fixed SMP is cooled down and the external force is released to form a temporary shape. Finally, the SMP is heated above phase transition temperature, the mobility of the polymer is increased and the polymer recovers its permanent shape. Usually the permanent shape of SMPs are prepared by heating the polymer and the crosslinking agent above the melting point to carry out crosslinking reaction in a mould and the initial state (so called permanent shape) can be obtained after one moulding cooling cycle. Utilizing this principle, the micro- and nanoscale dual roughness structure as a permanent shape can be formed by SMP during crosslinking reaction process. When the structure was deformed under external force, it can be recovered to its original shape by heating treatment.[41,42] However, superhydrophobic surfaces with self-healing ability that can recover the micro- and nanoscale roughness structures based on shape memory effect have been rarely reported.[32, 43]

In this study, mechanically stable and self-healing superhydrophobic surfaces have been formed via aerosol assisted chemical vapor deposition (AACVD) using epoxy resin and PDMS shape memory polymer. After depositing at a suitable dynamic temperature (from 290 to 350°C during the deposition at a rate of 3°C/min), micro-nano hierarchical roughness structures on the glass were formed. The roughness structure combined with the low surface energy substance, PDMS, imparted superhydrophobicity to the coated glass. The obtained superhydrophobic surfaces retained its water anti-wettability after being exposed to UV irradiation for 168 h, double tape peeling test for 200 cycles, sandpaper abrasion for 2 metres with 100 g weight loaded as well as immersion in strong acid/base for 72 h. In addition, the as-prepared superhydrophobic surfaces also showed self-healing properties. When the surface roughness structure was crushed and lost its superhydrophobicity, the surface could recover its micro-nano tier roughness structure to repair its water anti-wettability under heating. Hence, we report on a new scalable method, AACVD, to make large area self-healing superhydrophobic materials that recover their micro and nano scale roughness from a shape memory effect.

Experimental section

Materials

PDMS, Sylgard 184 Silicone Elastomer Kit with components of PDMS elastomer precursor and curing agent, were purchased from Univar Specialty Consumables. Diglycidyl ether of Bisphenol A (DGEBA), Neopentyl glycol diglycidyl ether (NGDE) and poly(propylene glycol)bis(2-amino-propyl) (D230) were purchased from Sigma Aldrich. Organic solvents, including ethanol and ethyl acetate, were purchased from Fisher Scientific UK. All chemicals were used without further purification. Standard microscope glass slides were purchased from VWR International, Inc. Micro-grained sandpaper (TUFBAK, ADALOX, P1000) was bought from Norton Company.

Fabrication of superhydrophobic $(EP/PDMS)_n$@glass

(1) PDMS elastomer precursor part-A (Sylgard 184 elastomer base, 2 g) and PDMS precursor Part-B (sylgard 184 curing agent, 0.2 g) were dissolved in 100 mL of ethyl acetate and magnetically stirred for 20 min at room temperature to form a transparent coating solution A. Epoxy resin (EP) solution B was prepared by adding 2.0 g DGEBA, 0.6 g NGDE and 0.94 g D230 into 100 mL of ethanol. Mixture B was magnetically stirred for 20 min before use.

Subsequently the reaction precursor solution C was formed by mixing solution A and B in same volume ratios. The EP and PDMS composites film were deposited on glass using a cold-walled horizontal-bed CVD reactor. The reactor was assembled in a top-down heating configuration, with the carbon heating block positioned above a plate (14.5 × 4 × 0.4 cm) supporting the glass. The distance between the carbon block and the substrate was 5 mm. A quartz tube was used to enclose the carbon block and substrates. Upon reaching the set reactor temperature, a precursor aerosol was generated by an ultrasonic humidifier (PIFCO, 25 W, 40 kHz), and then, the aerosol was transported to the heated substrate with N_2 (1 L/min) (Figure 1). The substrates coated with EP/PDMS films were handled in air after cooling under nitrogen.

(2) In a typical preparation process, the temperature of the reactor was first set to 290 ℃, then the deposition commenced, and the deposition temperature was set to increase from 290 to 350 ℃ during the deposition, at a rate of 3 ℃/min. Once the entire EP/PDMS precursor (20 mL, $V_{solution\ A} : V_{solution\ B} = 1 : 1$) had been aerosolised and completely reacted, the reactor temperature was cooled back down to 290 ℃, and the process was repeated again with the dynamic temperature control. The obtained glass sample was denoted as $(EP/PDMS)_n$@glass, where n represents the number of deposition cycles.

(3) In contrast, the same layer-by-layer deposition process was used to deposit pure EP and PDMS solution with 3 deposition cycles, the corresponding samples denoted as EP_3@glass, $PDMS_3$@glass respectively.

Characterization

The SEM images were studied under a JEOL JSM-6701F Field emission scanning electron microscope (SEM). Contact angle (CA) measurements were performed with an FTA-1000 drop shape instrument (First Ten Angstroms Inc.) at ambient temperature with 7 μL water droplet as the indicator. All the CAs were determined by averaging values measured at 6 different points on each sample surface. Sliding angle (SA) measurements were performed using the tilted drop method, with a water droplet size of 15 μL at least 6 different positions on each sample were tested. UV-vis spectra were recorded using a Shimadzu UV-2600 spectrometer single beam instrument over a range of 200-1000 nm wavelengths. ATR-FTIR measurements were taken over a range of 400-4000 cm^{-1} using a Platinum ATR (BRUKER) equipped with a single reflection diamond attachment. X-ray photoelectron spectroscopy (XPS) was carried out using a Thermo Scientific K-a photoelectron spectrometer. Atomic force microscopy (AFM) images were collected on Keysight 5600LS.

Mechanical robustness test

Mechanical durability tests were performed by using sandpaper abrasion. Typically, the sample was cut into 26 x 26 mm and placed onto the sandpaper (the grading of sandpaper is P1000) with the polymer film touching the sandpaper, then a 100 g weight (0.01MPa) was loaded on the middle of the sample. The sample was moved 25 cm across the sandpaper by an external force parallel to the substrate. The sample was rotated 90° clockwise after each abrasion to make sure the sample was abraded in all four directions. The CAs and SAs of the samples were taken after every 25 cm abrasion tests.

The durability of obtained samples was also evaluated by using tape peeling test. A common double-sided tape was used to investigate the adhesion between superhydrophobic EP and PDMS polymer films and the glass substrates, and the CAs and SAs were measured after every 20 cycles.

The pencil hardness was estimated as follows: a pencil with quantified hardness was pressed firmly on the surfaces while moving along the surface at a constant speed. The pencil formed a 45° angle with the surface.

Chemical stability

The coated glasses were subjected to a UV irradiation using an artificial light source (UV lamp, 365 nm, 3.7 mW cm^{-2}) for a week to evaluate the UV resistance. The distance between UV lamp and the sample was 20 cm. The CAs and SAs were measured after every 24 hours. The anti-corrosion test was performed by immersing the superhydrophobic surfaces in either hydrochloric acid solution or sodium hydroxide solution (either pH 1 or 14) for 72 h.

Self-healing property

Self-healing ability of crushed roughness structure: Firstly, the sample was cut into 1 × 1 × 0.4 cm, and then put into a pressure mold. Then the mold was mounted on the pressure machine, and making the sample surface deliberately pressed under a specific load 20 MPa for 5 min, which resulted in the collapse of the surface topographic features. After that, the surface was simply heated at different temperatures to investigate the self-healing property.

Results and discussion

Characterization of the AACVD modified glasses

In this study, superhydrophobic coatings on glass were prepared by aerosol-assisted chemical vapor deposition (AACVD) which is a specialised CVD technology which can be operated at ambient pressure.[44, 45] The precursor solution (epoxy resin and PDMS mixture solution) was first aerosolised using an ultrasonic humidifier and then transported to the heated reactor by nitrogen carrier gas

allowing deposition of the film onto the glass substrate, as shown in Figure 1. Once the vaporised precursor solution goes through the heated substrate, the solvent evaporates and the precursors react with each other, followed by deposition onto the substrate to form the desired film materials. Meanwhile, the waste products are carried away to the exhaust. With the increase of time, more and more precursors nucleate and aggregate together and finally result in the formation of a film. The obtained film covered the substrate totally and was well adhered due to the excellent bonding strength between the epoxy resin and substrates.

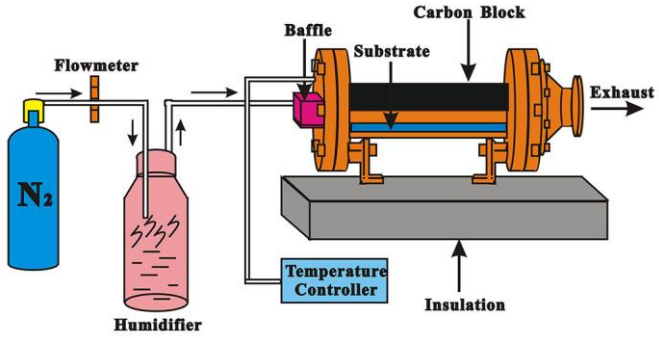

Figure 1. The illustration of principle of AACVD operation.

The deposition temperature is the most important factor for AACVD. In order to find out the influence of temperature on surface morphology and wettability, the EP and PDMS composite films (20 mL) were prepared at different fixed temperatures, and the corresponding SEM and contact angle images are shown in Figure 2(a-e). SEM images showed that the blank glass exhibited a flat and smooth surface. After being deposited with EP and PDMS composites at different temperature, the glass surface became much rougher than the blank one and was uniformly covered by many particles, indicating that the EP/PDMS composites had been successfully deposited onto the glass surface. Meanwhile, with increasing deposition temperature, the size of EP/PDMS particles decreased, with smaller size particles more likely to appear at higher temperature. This may due to the following reasons: (1) the curing process of EP and PDMS precursor, (2) the process of solvent volatilisation. High temperature is favourable for solidification of the precursor and volatilisation of the solvent. The obtained surfaces showed increasing static water CAs (102.3, 116.4, 124.1 and 133.5° at 290, 310, 330 and 350 °C, respectively) compared with blank glass (32.4°). The EP/PDMS films can also be prepared by a dynamic temperature control process and the corresponding surface morphology images and CA are shown in Figure 2 (f). The dynamic temperature control process was found to be more conduive to the formation of micro-nano roughness structures which is of benefit to the construction of superhydrophobic surfaces. By contrast, if using the epoxy resin precursor and PDMS cured directly, the contact angles of obtained surface was only 106.4 ± 2.4°.

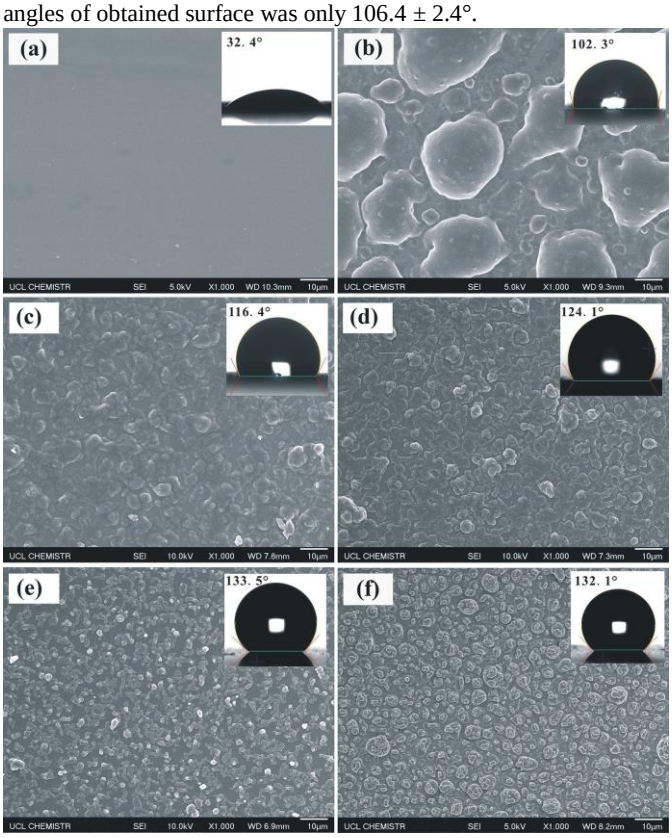

Figure 2. SEM and CAs images for different EP/PDMS@glass fabricated with different temperature: (a) Blank glass, (b) 290°C, (c) 310°C, (d) 330°C, (e) 350°C, (f) Deposited at Dynamic Temperature: the temperature was set to increase from 290 to 350 °C during the deposition at a rate of 3 °C/min.

In order to obtain superhydrophobic surfaces, the glass was treated to a layer-by-layer deposition method combined with a dynamic temperature control process. Figure 3(a) shows that the hydrophobicity of the film was dependent on the deposition cycles, and the CAs with water were stable and >150° when the deposition cycles exceeded 2. For deposition cycles over 3, the CA increased above 160° with a corresponding decrease of SA to <5°. Meanwhile, the CA and SA did not alter significantly after 3 deposition cycles, indicating saturation of hydrophobic moieties on the glass surfaces. These results indicate that when the volume ratio of EP and PDMS were constant, 3 deposition cycles was sufficient to convert the hydrophilic glass to superhydrophobic (Figure 3b) with CA of 163.9°±1.5° and SA of 1.7°±2° allowing water droplets to roll off easily. Figure 3(c) and (d) show the SEM images of $(EP/PDMS)_3$@glass. The 3 cycles layer-by-layer deposition resulted in dense and uniform coatings on the glass surface by EP/PDMS composites. The small size particles agglomerate into larger ones resulting in the surface becoming extremely rough (Figure 3e, Ra=611 nm). These micro scale structures combined with nano scale particles created a hierarchical roughness structure, which is very similar to the structure observed in a lotus leaf and allows for the formation of a superhydrophobic surface. By contrast, the surface

morphology of EP_3@glass showed that micro sized particles were stacked into flower-like particles, and the corresponding CA was 64.5° (Figure S1a). Figure S1 (b) showed that the surface of $PDMS_3$@glass was covered by particles with different size, and the surface CA was 137.8°. These results all indicate that the combination of hierarchical roughness structure and low surface energy materials is beneficial to the construction of superhydrophobic surface. Meanwhile, as seen from the cross-sectional SEM of the sample films fabricated in the Figure S3, with the deposition cycles increased, the thickness of the films increased and the increase of the film thickness was almost linear with the deposition cycles (see Figure S4). We also investigated the relationship between the deposition cycles and the transparency of $(EP/PDMS)_n$@glass. With an increase in deposition cycles, the transparency of the obtained glass sharply decreased. The sample deposited for 1 cycle had the best transparency but the lowest water contact angle. While the sample deposited for 5 cycles showed the lowest transparency, indicating the thickest and densest film (Figure S2). This film gives excellent superhydrophobic properties with a high water contact angle and low sliding angle.

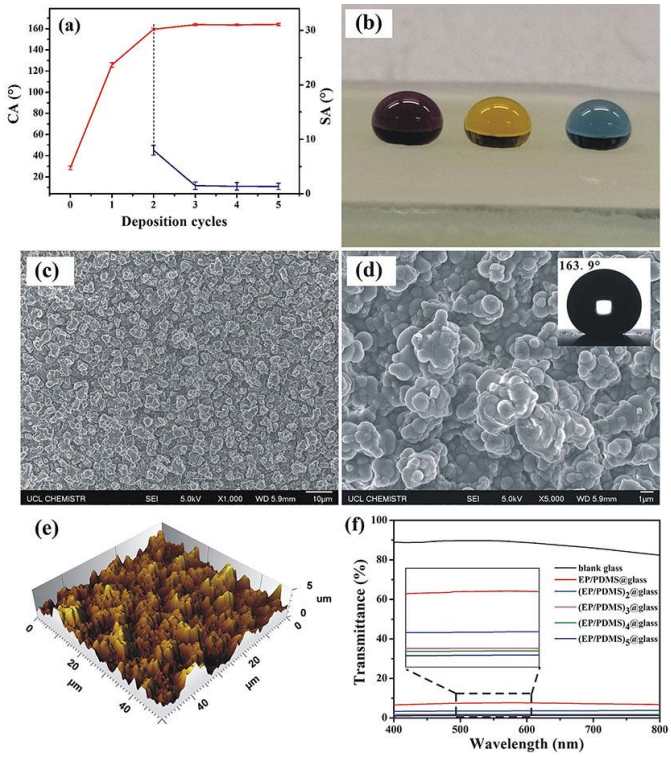

Figure 3. (a) The relationship between the CA/SA of $(EP/PDMS)_n$@glass and deposition cycles, where n represents deposition cycles, (b) Digital image of dyed water droplets after contacting $(EP/PDMS)_3$@glass, (c) SEM image of $(EP/PDMS)_3$@glass, (d) Higher magnification of (c), (e) AFM image of $(EP/PDMS)_3$@glass, Ra=611 nm. (f) The transparency on blank glass and the as-prepared $(EP/PDMS)_n$@glass surfaces with different deposition cycles.

It's worth mentioning that this facile route is scalable[46] and can also be applied to various substrates including flexible materials such as paper and copper mesh and hard materials such as aluminum plate at same deposition condition. Figure S2 shows the water contact images for different substrates. The optical images of dyed water droplets on the substrate indicated that superhydrophobicity has been successfully obtained. But in this paper, we used glass as the final substrate, all the characterization, stability and self-healing test were performed on the obtained $(EP/PDMS)_3$@glass.

The chemical composition of the glass surface was analysed by XPS and the result is shown in Figure 4(a). The surface of the blank glass showed C 1s, O 1s, Si 2s, Si 2p, and Ca 3p, Ca 2p signals, while the surface of $(EP/PDMS)_3$@glass was dominated by a new N 1s signal and the Ca 3p, Ca 2p signals were no longer observed. This demonstrated that EP/PDMS composites were successfully deposited onto the glass surface. The FT-IR spectra of EP_3@glass, $PDMS_3$@glass and the correspondingly modified $(EP/PDMS)_3$@glass are shown in Figure 4(b). The peak at 2960-2850 cm^{-1} corresponded to the $-CH_2$, $-CH_3$ stretching vibration absorption, 1380 and 1460 cm^{-1} were due to the bending vibration absorption, while the peak observed at 1620, 1580 and 1500 cm^{-1} represented the benzene skeleton vibration absorption. The absorption signal observed at 1100 and 1240 cm^{-1} corresponded to the C-O-C stretching vibration. The peak at 1200 cm^{-1} represented the =C-O of the phenol, whereas the peaks at 1030 and 894 cm^{-1} could be attributed to the C-N stretching and bending vibration of the tertiary amine group. The peak at 804 cm^{-1} was attributed to the para substitution of benzene. All the above characteristic peaks confirm that epoxy resin is a kind of phenolic polymer containing tertiary amine group. In comparison with the FT-IR spectrum of $(EP/PDMS)_3$@glass, the spectrum displayed several additional absorption peaks at 864 and 740 cm^{-1}, which are consistent with $Si(CH_3)_2$ stretching vibration of PDMS suggesting that the EP/PDMS composite was successfully loaded on to the glass surface.

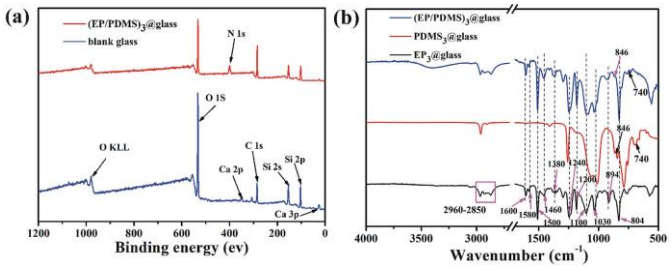

Figure 4. (a) XPS spectra of the blank glass and (EP/PDMS)3@glass, (b) FT-IR spectra of EP3@glass, PDMS3@glass, (EP/PDMS)3@glass.

Stability of the superhydrophobic $(EP/PDMS)_3$@glass

The influence of the ambient force on the stability and robustness of superhydrophobic surfaces is one of the most important factors that must be considered for daily applications. Such resistance against mechanical damage was evaluated by abrading samples of the $(EP/PDMS)_3$@glass using sandpaper with a 100 g weight loaded. It was found that the CAs decreased from 163.9 ± 1.5° to 158.7 ± 2.3° and changed only slightly after an abrasion distance of 2 m. The SA

increased from 1.7 ± 1° to 5.4 ± 2.4°, as shown in Figure 5(a). There are two reasons for this phenomenon. Firstly, as the abrasion length increased, the roughness on the $(EP/PDMS)_3$@glass surface decreased (Figure 5b) due to the mechanical action. Secondly, with the abrasion length increased, the thickness of EP/PDMS films were reduced under such severe mechanical abrasion. These can be indicated from the cross-sectional SEM images shown in Figure S5(b), the film thickness were reduced from 11.2 to 4.3 μm after 2 m sandpaper abrasion. However, the surface rough structures remained enabling retention of the superhydrophobicity (See Figure 6b).

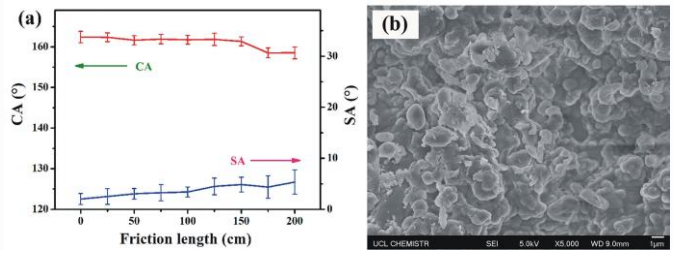

Figure 5. (a) Changes of CAs and SAs of $(EP/PDMS)_3$@glass with friction length. (b) SEM image of $(EP/PDMS)_3$@glass after 2 m sandpaper abrasion distance.

In order to further measure the durability against mechanical stress, a procedure of tape peeling test experiments was performed on the samples of $(EP/PDMS)_3$@glass by using a commercial double sided tape which was repeatedly stuck to the EP/PDMS film surface and removed. The CAs and SAs were measured after every 20 cycles and the results are shown in Figure 6. It was found that the CAs of the $(EP/PDMS)_3$@glass decreased from 163.9 ± 1.5° to 157 ±3°, whereas the SA increased from 1.7 ± 1° to 4.9 ± 2° (Figure 6a). The SEM image, as shown in Figure 6(b), shows that the surface morphology of the film was not destroyed although the thickness of the film was reduced to 4.4 μm, indicating excellent durability of superhydrophobicity against tape peeling.

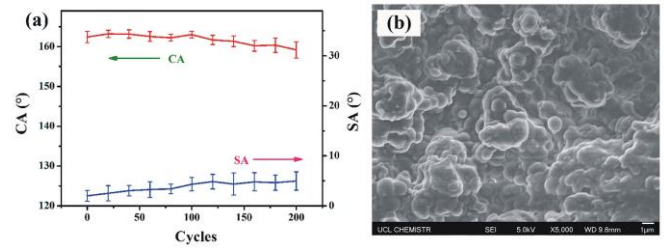

Figure 6. (a) Changes of CAs and SAs of $(EP/PDMS)_3$@glass with tape peeling cycles, (b) SEM image of $(EP/PDMS)_3$@glass after 200 cycles tape peeling test.

The EP/PDMS composites also retained excellent film-forming properties and showed high adhesion to glass, displaying good resistance not only to sandpaper abrasion and double-sided tape peeling, but also to knife scratching. The $(EP/PDMS)_3$@glass was scratched by a knife, as can be seen in Figure S3. After knife scraping, obvious scratches were apparent on the surface although the EP/PDMS composites were not removed completely and the surface CA did not significantly change. However, if the scratched surface was further treated to peeling off with double side tape, the surface CA decreased to 146.8°, which may be due to the removal of hydrophobic material from the scratched edges by the double-sided tape, as shown in Figure S3b.

Meanwhile, a pencil hardness test was also performed to evaluate the mechanical robustness of the film. It is generally known that a good index of performance for a durable superhydrophobic surface is at least 2H [47]. The pencil hardness test in this paper was conducted as follows according to a modified previous work [48]: A pencil with a quantified hardness was pressed firmly on the surface while moving along it at a constant speed. The pencil forms a 45° angle with the surface and was loaded with an applied force of 10 N. The SEM images in Fig. 10(a) and (b) show that most of the nanoparticles were still attached to the surface after 2H, 3H and 4H pencil hardness tests, and the surface contact angles were still above 150°, indicating that the superhydrophobic film can withstand the 4H pencil hardness test. But, the surface can not withstand a 5H pencil hardness test, in which the polymer films were almost removed and the surface contact angle decreased to 138.5°.

The obtained superhydrophobic $(EP/PDMS)_3$@glass surface showing excellent mechanical stability can be attributed to two factors. Epoxy resin polymer contains a large number of extremely active groups, such as epoxy groups, hydroxyl groups, ether groups and amine groups. These polar groups can not only form hydrogen bonds with substrate surface, impart high viscosity between epoxy resin and substrate surface, but also can form chemical bond with glass. It is well known that as a kind of silicone elastomer, PDMS can be cured to form a crosslinked rubber showing excellent durability due to reformation of the elastomer PDMS coating can rebound after the load is withdrawn [14, 49].

The chemical stability and robustness of the obtained surfaces were evaluated based on variation of changes in the water repellency of $(EP/PDMS)_3$@glass. The samples were dipped in solution with different pH values (pH 1-14) for 72 h. Figure 7(a) shows that the CA of the superhydrophobic surface were not significantly changed, indicating strong resistance to different pH solutions. This phenomenon may be due to the air layer trapped on the surface which can inhibit the attack of acid or alkali.[21] We also estimated the stability of the obtained samples after immersed in different pH solution for 30 days, as shown in Figure S8. After 30 days immersion, the CAs of the surfaces were still above 150°, indicating that the surfaces were stable to different pH solution. Figure 7(b) shows the CAs and SAs of $(EP/PDMS)_3$@glass surface as a function of UV irradiation time. The CA increased slightly from 163.9 ± 1.5° to 165.3 ± 1° after the first 6 h, possibly due to the migration of hydrophobic molecule chains caused by the heating effect under UV irradiation. Prolonging the irradiation time to 168 h, the CA and SA showed no great change, indicating excellent resistance of the $(EP/PDMS)_3$@glass to UV light. However, the CA decreased from 163.9 ± 1.5° to 155.7 ± 2.3° with SA increased from 1.7 ± 1° to 6.4 ± 2.4° after further irradiation of 720 h, this might be because some C-C bonds were broken down forming polar groups. However, the

surface superhydrophpbicity was still maintained, showing excellent stability to UV irradiation.

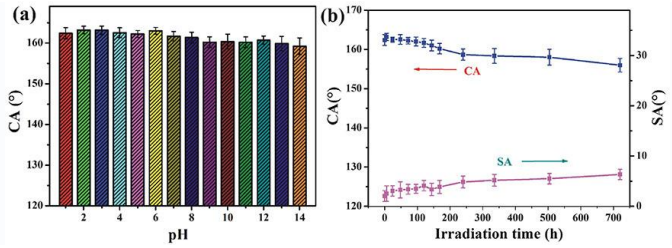

Figure 7. (a) CAs of the $(EP/PDMS)_3$@glass treated by immersion in different pH solution; (b) Changes of CAs and SAs of $(EP/PDMS)_3$@glass with different irradiation time.

Self-healing properties.

The self-healing ability of the as-prepared $(EP/PDMS)_3$@glass surface was investigated by deliberately pressing the samples under an external load to destroy the surface morphology. As it is shown in Figure 8, after pressing, the surface became relatively flat. Instead of dense clusters of particles, the surface was covered with new indentations. Meanwhile, the surface superhydrophobicity disappeared, and the water contact angle of the surface was reduced to about 116.3°. It should be noted that the surface chemical composition had no obvious change during the pressing process, indicating that the loss of superhydrophobicity was the result of the destruction of the surface hierarchical structures. However, after heating at 85 ℃ for 2 min, the crushed roughness structures were nearly completely recovered. In addition, the restored surface morphology was very similar to the original surface. More importantly, the surface recovered its low-adhesive superhydrophobicity, the CA and SA were 163.1° and 0.9° respectively.

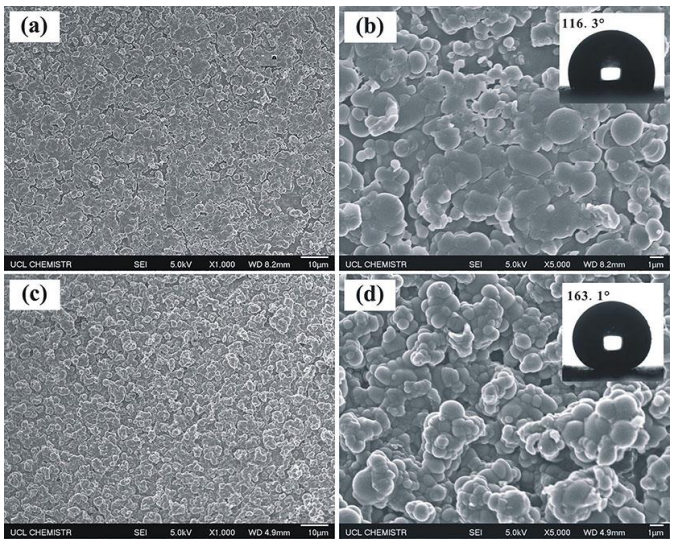

Figure 8. The surface morphologies of (a)(b) crushed $(EP/PDMS)_3$@glass after application of an external force, (c)(d) Self-healing $(EP/PDMS)_3$@glass after healing at 85°C.

In order to further demonstrate the change of pristine, crushed and recovered $(EP/PDMS)_3$@glass, the morphologies of the corresponding $(EP/PDMS)_3$@glass were investigated by AFM, which are shown in Figure 9. The surface roughness value, Ra of the pristine $(EP/PDMS)_3$@glass surface (Figure 9a) was 611 nm. However, after pressing under a certain external force, the surface roughness value, Ra of the crushed $(EP/PDMS)_3$@glass surface (Figure 9b) was decreased to 313 nm, which was much lower than the corresponding value of the pristine $(EP/PDMS)_3$@glass surface. However, after heating the crushed $(EP/PDMS)_3$@glass at 85°C for 5 min, the surface roughness value Ra was recovered to 582 nm, which was similar to the pristine surface, indicating nearly complete recovery of the surface roughness.

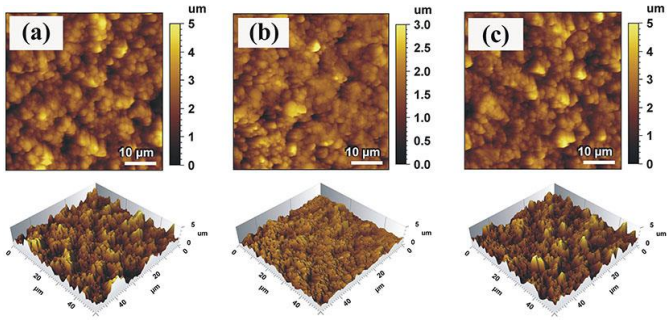

Figure 9. AFM images of (a) Pristine $(EP/PDMS)_3$@glass, Ra=611 nm; (b) Crushed $(EP/PDMS)_3$@glass, Ra=313 nm; (c) Recovered $(EP/PDMS)_3$@glass, Ra=582 nm.

As shown in Figure 10(a), this pressing-healing process can be repeated at least 10 times without apparently decreasing the superhydrophobicity of the self-healed $(EP/PDMS)_3$@glass. The SEM images confirm that the film still has the micro and nano-scaled hierarchical structure that are essential to superhydrophobicity after several pressing-healing cycles. In addition, the recovery velocity can also be increased by increasing the heating temperature when the crushed $(EP/PDMS)_3$@glass was heated at different temperatures for 2 min, such as 45, 65, 85, 105 and 125°C respectively.

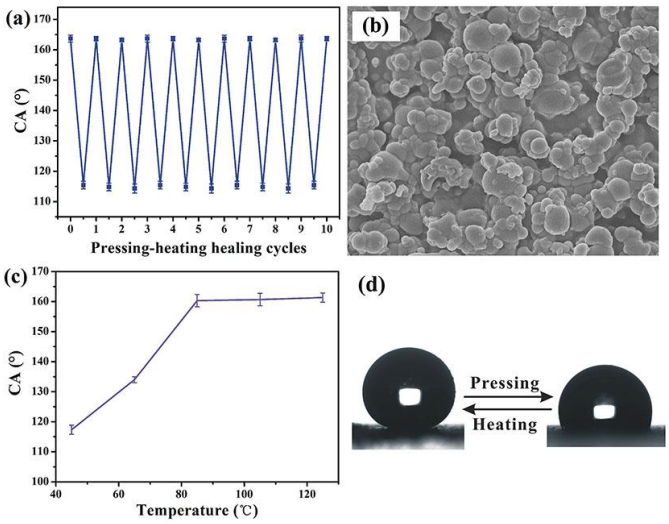

Figure 10. (a) Self-healing cycles of the $(EP/PDMS)_3$@glass treated at 85°C. (b) SEM image of $(EP/PDMS)_3$@glass after 7 pressing-healing cycles. (c) CAs of crushed $(EP/PDMS)_3$@glass after heating at different temperature for 2 min. (d) Reversible transition between superhydrophobic (left) and hydrophobic (right) states of $(EP/PDMS)_3$@glass surface upon external load treating and self-healing process.

The self-healing ability of the as-prepared (EP/PDMS)$_3$@glass surface can be ascribed to the shape memory effect of the polymer (Figure S10 and table S1). The chemical structures of the reactants used in our epoxy formulation are shown in Figure S9 . The molar ratio of the liquid epoxy resin precursor (DGEBA/NGDE/D230 = 2 : 1 : 3, the corresponding mass were 2.0 g GDEBA, 0.6 g NGDE and 0.94 g D230) used here can form a kind of heat-induced SMP, which can memorise and recover their permanent shape under heat treatment to induce a shape memory effect (Figure S11). In the process of AACVD, the epoxy resin precursor DGEBA was reacted with D230 and NGDE by epoxy and amino groups to form network structure epoxy polymer. As a hydrophobic materials, PDMS was mixed with epoxy polymers and interspersed into the network structure of epoxy polymers, and then the mixed polymer would be cross-linked, cured, and deposited onto the glass to form a film with micro-nano scale rough structures. As for the obtained films, these hierarchical rough structures were the permanent shape. In such state, the molecule network of the polymer film was in the dynamically and thermodynamically stable state and the surface showed low-adhesive superhydrophobicity, demonstrating a Cassie-Baxter type surface. When the surface was pressed under external force, the surface roughness structure collapsed, and the molecule network reaches a thermodynamically unstable but dynamically stable state. The polymer molecule chains were in a non-equilibrium state, the molecule network reached a thermodynamically unstable but dynamically stable state. As a result, the surface loses its superhydrophobicity. After heating, however, the mobility of the polymer chains increased allowing the molecule conformation to change back to its original permanent conformation, and thus achieved the restoration of the surface roughness structure. Finally, after cooling to room temperature, the surface microstructure and related original superhydrophobicity was restored, as shown in Figure 11.

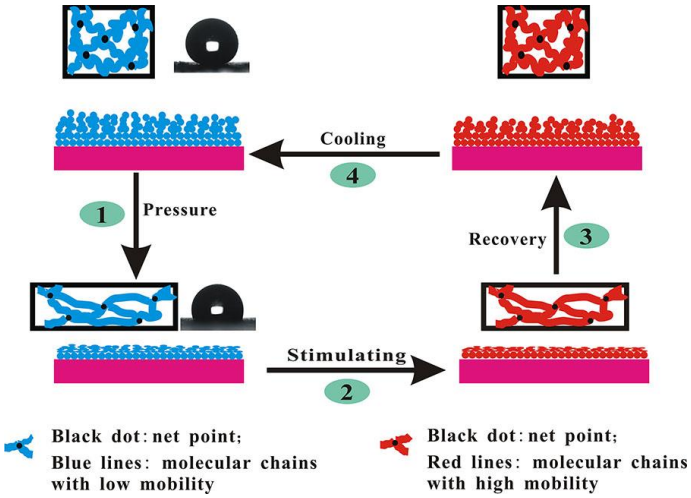

Figure 11. Schematic illustration of the self-healing process.

In order to further illustrate the self-healing ability of (EP/PDMS)$_3$@glass mainly came from shape memory epoxy resin, the corresponding EP$_3$@glass and PDMS$_3$@glass were pressed under the same external force, and then the pressed samples were heated at 85 ℃ for 5 min. As shown in Figure S12, there were indentations on the surface after pressing EP$_3$@glass and PDMS$_3$@glass. After heating, the epoxy resin film recovered its original surface morphology. However, there was no change between crushed PDMS$_3$@glass and heated PDMS$_3$@glass, indicating that the PDMS$_3$@glass has no self-healing ability.

Conclusions

In summary, we have demonstrated a simple and novel strategy to prepare mechanically robust and self-healing superhydrophobic surfaces via aerosol-assisted layer-by-layer CVD of epoxy resin and PDMS. It was shown that the excellent adhesion of epoxy resin in combination with PDMS elastomer made the superhydrophobic surfaces resistant to UV irradiation, chemical etching, double tape peeling, sandpaper abrasion and knife scratching. Importantly, the surface superhydrophobicity could be simply recovered by heating if the surfaces hierarchical roughness structures were destroyed by external pressure. This method might be suitable for other substrates for fabrication of superhydrophobic surfaces, paving a way for generating large-scale production of robust and self-healing superhydrophobic surfaces through AA-LbL-CVD.

Acknowledgements

The authors acknowledge the National Natural Science Foundation of China (51572161) for financial support. X. -J. Guo and J. Guo are thankful for the funding from the China Scholarship Council (CSC). C. J. Carmalt, I. P. Parkin, K. Page. and F. L. Heale acknowledge AzkoNobel, Innovate UK (192541) and EPSRC for a studentship (FLH) through the Molecular Modelling and Materials Science Doctoral Training Centre (EP/L015862/1) and funding (EP/N510051).

Notes and references

1. L. Xu, G. Xiao, C. Chen, R. Li, Y. Mai, G. Sun and D. Yan, *Journal of Materials Chemistry A*, 2015, **3**, 7498-7504.
2. H. Wang, E. Wang, Z. Liu, D. Gao, R. Yuan, L. Sun and Y. Zhu, *Journal of Materials Chemistry A*, 2015, **3**, 266-273.
3. D. Ge, L. Yang, C. Wang, E. Lee, Y. Zhang and S. Yang, *Chemical Communications*, 2015, **51**, 6149-6152.
4. Y. Si, Q. Fu, X. Wang, J. Zhu, J. Yu, G. Sun and B. Ding, *ACS Nano*, 2015, **9**, 3791-3799.
5. S.-M. Kang, S. Hwang, S.-H. Jin, C.-H. Choi, J. Kim, B. J. Park, D. Lee and C.-S. Lee, *Langmuir*, 2014, **30**, 2828-2834.
6. X. Kong, J. Zhang, Q. Xuan, J. Lu and J. Feng, *Langmuir*, 2018, **34**, 8294-8301.

7. C.-H. Xue, X.-J. Guo, J.-Z. Ma and S.-T. Jia, *ACS Applied Materials & Interfaces*, 2015, **7**, 8251-8259.
8. A. M. Emelyanenko, L. B. Boinovich, A. A. Bezdomnikov, E. V. Chulkova and K. A. Emelyanenko, *ACS Applied Materials & Interfaces*, 2017, **9**, 24210-24219.
9. L. B. Boinovich, A. M. Emelyanenko, K. A. Emelyanenko and K. I. Maslakov, *Physical Chemistry Chemical Physics*, 2016, **18**, 3131-3136.
10. L. Wang, Q. Gong, S. Zhan, L. Jiang and Y. Zheng, *Advanced Materials*, 2016, **28**, 7729-7735.
11. Y. Shen, J. Tao, H. Tao, S. Chen, L. Pan and T. Wang, *Langmuir*, 2015, **31**, 10799-10806.
12. M. Ruan, W. Li, B. Wang, B. Deng, F. Ma and Z. Yu, *Langmuir*, 2013, **29**, 8482-8491.
13. B. Deng, R. Cai, Y. Yu, H. Jiang, C. Wang, J. Li, L. Li, M. Yu, J. Li, L. Xie, Q. Huang and C. Fan, *Advanced Materials*, 2010, **22**, 5473-5477.
14. H. Zhou, H. Wang, H. Niu, A. Gestos, X. Wang and T. Lin, *Advanced Materials*, 2012, **24**, 2409-2412.
15. J. Li, L. Li, X. Du, W. Feng, A. Welle, O. Trapp, M. Grunze, M. Hirtz and P. A. Levkin, *Nano Letters*, 2015, **15**, 675-681.
16. Y. Wang, Y. Shi, L. Pan, M. Yang, L. Peng, S. Zong, Y. Shi and G. Yu, *Nano Letters*, 2014, **14**, 4803-4809.
17. C.-H. Xue and J.-Z. Ma, *Journal of Materials Chemistry A*, 2013, **1**, 4146-4161.
18. S. S. Latthe, P. Sudhagar, A. Devadoss, A. M. Kumar, S. Liu, C. Terashima, K. Nakata and A. Fujishima, *Journal of Materials Chemistry A*, 2015, **3**, 14263-14271.
19. F. Su and K. Yao, *ACS Applied Materials & Interfaces*, 2014, **6**, 8762-8770.
20. N. Wang, D. Xiong, Y. Deng, Y. Shi and K. Wang, *ACS Applied Materials & Interfaces*, 2015, **7**, 6260-6272.
21. C.-H. Xue, X.-J. Guo, M.-M. Zhang, J.-Z. Ma and S.-T. Jia, *Journal of Materials Chemistry A*, 2015, **3**, 21797-21804.
22. A. Zhuang, R. Liao, Y. Lu, S. C. Dixon, A. Jiamprasertboon, F. Chen, S. Sathasivam, I. P. Parkin and C. J. Carmalt, *ACS Applied Materials & Interfaces*, 2017, **9**, 42327-42335.
23. S. Li, K. Page, S. Sathasivam, F. Heale, G. He, Y. Lu, Y. Lai, G. Chen, C. J. Carmalt and I. P. Parkin, *Journal of Materials Chemistry A*, 2018, **6**, 17633-17641.
24. K. Chen, S. Zhou, S. Yang and L. Wu, *Advanced Functional Materials*, 2015, **25**, 1035-1041.
25. Y. Si, H. Zhu, L. Chen, T. Jiang and Z. Guo, *Chemical Communications*, 2015, **51**, 16794-16797.
26. Y. Li, Y. Zhao, X. Lu, Y. Zhu and L. Jiang, *Nano Research*, 2016, **9**, 2034-2045.
27. Q. Liu, X. Wang, B. Yu, F. Zhou and Q. Xue, *Langmuir*, 2012, **28**, 5845-5849.
28. M. Wu, B. Ma, T. Pan, S. Chen and J. Sun, *Advanced Functional Materials*, 2016, **26**, 569-576.
29. Y. Li, L. Li and J. Sun, *Angewandte Chemie*, 2010, **122**, 6265-6269.
30. H. Wang, Y. Xue, J. Ding, L. Feng, X. Wang and T. Lin, *Angewandte Chemie International Edition*, 2011, **50**, 11433-11436.
31. C.-H. Xue, Z.-D. Zhang, J. Zhang and S.-T. Jia, *Journal of Materials Chemistry A*, 2014, **2**, 15001-15007.
32. U. Manna and D. M. Lynn, *Advanced Materials*, 2013, **25**, 5104-5108.
33. K. Chen, S. Zhou and L. Wu, *Chemical Communications*, 2014, **50**, 11891-11894.
34. N. Puretskiy, G. Stoychev, A. Synytska and L. Ionov, *Langmuir*, 2012, **28**, 3679-3682.
35. A. Das, J. Deka, K. Raidongia and U. Manna, *Chemistry of Materials*, 2017, **29**, 8720-8728.
36. Y. Wu, J. Hu, C. Zhang, J. Han, Y. Wang and B. Kumar, *Journal of Materials Chemistry A*, 2015, **3**, 97-100.
37. Z. Feng, J. Hu, H. Zuo, N. Ning, L. Zhang, B. Yu and M. Tian, *ACS Applied Materials & Interfaces*, 2018.
38. A. C. Weems, W. Li, D. J. Maitland and L. M. Calle, *ACS Applied Materials & Interfaces*, 2018, **10**, 32998-33009.
39. L. Zhao, L. Zhang, J. Zhao, J. Shi, Z. Dai, G. Wang, C. Zhang, B. Li, X. Feng, H. Zhang, J. Zhang and Z. Zhang, *ACS Applied Materials & Interfaces*, 2018.
40. L. Yu, Q. Wang, J. Sun, C. Li, C. Zou, Z. He, Z. Wang, L. Zhou, L. Zhang and H. Yang, *Journal of Materials Chemistry A*, 2015, **3**, 13953-13961.
41. T. Lv, Z. Cheng, D. Zhang, E. Zhang, Q. Zhao, Y. Liu and L. Jiang, *ACS Nano*, 2016, **10**, 9379-9386.
42. J. H. Lee, R. Hinchet, S. K. Kim, S. Kim and S.-W. Kim, *Energy & Environmental Science*, 2015, **8**, 3605-3613.
43. T. Lv, Z. Cheng, E. Zhang, H. Kang, Y. Liu and L. Jiang, *Small*, 2017, **13**, 1503402.

44. S. Ponja, S. Sathasivam, N. Chadwick, A. Kafizas, S. M. Bawaked, A. Y. Obaid, S. Al-Thabaiti, S. N. Basahel, I. P. Parkin and C. J. Carmalt, *Journal of Materials Chemistry A*, 2013, **1**, 6271-6278.

45. E. Ozkan, C. C. Crick, A. Taylor, E. Allan and I. P. Parkin, *Chemical Science*, 2016, **7**, 5126-5131.

46. M. J. Powell, D. B. Potter, R. L. Wilson, J. A. Darr, I. P. Parkin and C. J. Carmalt, *Materials & Design*, 2017, **129**, 116-124.

47. A. Milionis, E. Loth and I. S. Bayer, *Advances in Colloid and Interface Science*, 2016, **229**, 57-79.

48. M. Xu, Y. Feng, Z. Li, X. Wang, C. Li, H. Jiang and Y. Chen, *Journal of Alloys and Compounds*, 2019, **781**, 1175-1181.

49. C.-H. Xue, Y.-R. Li, P. Zhang, J.-Z. Ma and S.-T. Jia, *ACS Applied Materials & Interfaces*, 2014, **6**, 10153-10161.